Journal of Power Sources 269 (2014) 266–273

Contents lists available at ScienceDirect

Journal of Power Sources

journal homepage: www.elsevier.com/locate/jpowsour

On the origin of the capacity fading for aluminium negative electrodes in Li-ion batteries

Gabriel Oltean [a], Cheuk-Wai Tai [b], Kristina Edström [a], Leif Nyholm [a, *]

[a] Department of Chemistry, Ångström Laboratory, Uppsala University, Box 538, SE-75121, Uppsala, Sweden
[b] Department of Materials and Environmental Chemistry, Arrhenius Laboratory, Stockholm University, SE-10691, Stockholm, Sweden

HIGHLIGHTS

- The capacity loss for aluminium nanorod anodes is due to lithium trapping.
- The capacity loss is controlled by the diffusion of lithium in the aluminium.
- Very good cycling stability was seen between 0.1 and 1 V vs. Li^+/Li.
- The cycling performance was not affected by the alumina layer thickness.
- Volume expansion effects do not explain the cycling behaviour.

ARTICLE INFO

Article history:
Received 25 April 2014
Received in revised form
9 June 2014
Accepted 22 June 2014
Available online 7 July 2014

Keywords:
Aluminium
Nanorods
Li-ion battery anode
Capacity loss
Diffusion
Volume expansion

ABSTRACT

The origin of the capacity loss for aluminium negative electrodes in Li-ion batteries has been studied for electrodeposited aluminium nanorod electrodes coated with Al_2O_3 layers of different thicknesses (i.e. a native oxide layer, 30 and 60 nm) mainly employing pouch cell voltammetric cycling versus metallic lithium. Whereas the capacity decreased continuously during cycling between 0.1 and 3 V vs. Li^+/Li, good cycling stability was obtained when the cycling was carried out between 0.1 and 1 V vs. Li^+/Li. Since no significant dependence of the cycling stability on the thickness of the alumina layer was found in any of the experiments, the observed loss of capacity is unlikely to have been caused by volume expansion effects. The latter is further supported by the finding that the capacity (obtained when cycling between 0.1 and 3 V vs. Li^+/Li) decreased linearly with the inverse of the square root of the cycling time, indicating that the capacity loss was due to the loss of lithium as a result of lithium diffusion into the bulk of the aluminium electrodes. The latter is explained based on a lithium-aluminium alloying and dealloying model which complements previously published models.

1. Introduction

Aluminium is widely used as the positive electrode current collector in Li-ion batteries since it is corrosion resistant, light and relatively inexpensive. As aluminium forms an alloy with lithium at a potential close 0 V vs. Li^+/Li, aluminium could in principle also be used as a negative electrode material [1]. This would facilitate the manufacturing of Li-ion batteries significantly as aluminium then could be used both as the positive current collector and as a combined negative current collector and electrode. At present, significant research efforts are made to enable a replacement of the commercially employed graphite negative electrode material with higher capacity metals or metal oxides [2]. In this quest, silicon and tin have received a lot of attention since they can form alloys with up to 4.4 Li atoms per metal atom and therefore provide high gravimetric as well as volumetric specific capacities. During the alloying and dealloying with lithium, Si and Sn electrodes, however, experience significant volume changes of the order of 300–400% which generally give rise to capacity losses upon cycling. In analogy with silicon and tin, aluminium also forms alloys with lithium although the reaction in this case generally is assumed to involve only one lithium atom per aluminium atom, yielding a theoretical capacity of about 1000 mAh g^{-1} and a volume expansion of less than 100%.

The use of aluminium as a negative electrode material in Li-ion cells, however, suffers from poor coulombic efficiencies and rapid capacity fading upon cycling. This capacity fading, which generally is most pronounced during the first few cycles, is currently mainly

* Corresponding author. Tel.: +46 (0)184713742; fax: +46 (0)18513548.
E-mail address: leif.nyholm@kemi.uu.se (L. Nyholm).

http://dx.doi.org/10.1016/j.jpowsour.2014.06.118
0378-7753/

ascribed to volume expansion effects although the experimental support for this conclusion is less convincing for aluminium than for silicon and tin, at least for electrodes of conventional dimensions. Conflicting conclusions regarding the origin of the capacity loss for aluminium negative electrodes during cycling can also be found in the literature, particularly when comparing contemporary and older publications.

In attempts to investigate the capacity loss upon cycling, aluminium negative electrodes have been studied by many groups [3–29] employing different electrode preparation and characterisation approaches during more than four decades. The influence of particle size [3–5], crystal orientation [6] and electrode morphology [7] on the cycling performance of aluminium electrodes have thus been studied but the results are unfortunately contradictory. The use of an inactive component in the aluminium matrix [8,9] or a buffer layer [10] covering the aluminium particles have likewise been investigated without significant success.

The performance of aluminium nanorod or nanowire negative electrodes in Li-ion batteries has also been studied by several groups [11–13]. Zein El Abedin et al. [11] synthesised aluminium nanowires which were cycled for 50 cycles and which showed no significant capacity loss during the first four cycles in contrary to other published results [12,13]. Recently, Liu et al. [14] described an *in situ* TEM study of aluminium nanowires indicating that the aluminium alloying and dealloying processes give rise to isolated aluminium nanoparticles underneath the native alumina oxide layer even though the structural integrity of the nanowire was maintained. Based on the latter results it is tempting to conclude that the capacity losses seen for aluminium electrodes mainly stem from a loss of electrical contact to parts of the electrode as a result of the stress caused by the volume changes as for silicon and tin electrodes.

Even though volume expansion effects may limit the cycling stability of aluminium electrodes, an examination of the older literature clearly shows that the cycling stability of aluminium electrodes is affected by at least one other effect since the cycling ability also has been reported to be limited by a loss of lithium in the aluminium electrode [15–29]. This poor capacity retention of aluminium electrodes has been ascribed to lithium trapping in the aluminium electrode during cycling [15–17]. It has, however, also been found that aluminium electrodes can be efficiently cycled provided that a certain degree of alloying of the aluminium electrodes is achieved and that only about 2% of the capacity is used in the cycling [18,19]. The cycling efficiency of the aluminium negative electrodes has likewise been found to depend on the current density, the cycled charge [20] and the pretreatment of the electrodes [21]. Although Li_3Al_2 and Li_9Al_4 alloys were expected to form during lithiation of the aluminium electrode [15,16], only the LiAl phase was observed experimentally using X-Ray diffraction [22]. The nucleation and 3-D growth process involved in the formation of the alloy between aluminium and lithium has also been studied in detail [23].

Three decades ago, Owen and co-workers [24,25] proposed a model in which a growing layer of β-LiAl is formed on aluminium electrodes during the lithiation process while the delithiation reaction gives rise to a trapped β-LiAl layer between two lithium deficient layers. In this model, a lower diffusion coefficient for lithium in the Li poorer α-LiAl phase (10^{-11} cm^2 s^{-1} [26]) than in the β-LiAl phase (10^{-8}–10^{-9} cm^2 s^{-1} [27,28]) was used to explain the fact that columbic efficiencies significantly below 100% generally were obtained on the first cycles. More recently, Ui et al. [29] studied the concentration profiles of lithium within aluminium electrodes and demonstrated that lithium was indeed present within the electrodes even after the dealloying step. The latter authors also showed that the lithiation and delithiation charge for an aluminium electrode increased with the cycle number in cyclic voltammetry experiments in the potential region between 0 and 2.4 V vs. Li^+/Li.

At present there are consequently two main hypotheses regarding the origin of the capacity losses seen for aluminium negative electrodes in Li-ion batteries. Although the discussion at present mainly is focused on volume expansion effects, losses of lithium in the aluminium electrode should clearly also be taken into consideration which is why there is thus a need for studies in which the cycling performance of aluminium electrodes is evaluated based on these two hypotheses. Another issue that so far has received very little attention is the influence of the native alumina layer on the performance of aluminium electrodes in Li-ion batteries. Although it is known that thin alumina layers can be used to minimize the effects of volume changes for alloying electrodes [30,31], the effect of such layers on the cycling stability of aluminium electrodes has not been investigated systematically. If the capacity loss of aluminium electrodes is indeed due to volume expansion effects it would be anticipated that these problems could be circumvented by the use of aluminium electrodes coated with sufficiently thick alumina layers.

In the present work, the cycling performance of aluminium nanorod electrodes covered with a native layer of alumina, as well as with 30 nm and 60 nm thick alumina layers, respectively are discussed. The obtained dependence of the capacity on the cycle number is examined on the basis of the volume expansion and lithium loss hypotheses mainly employing cyclic voltammetric data obtained in different potential windows. Based on the obtained results, a model for the alloying and dealloying processes for aluminium electrodes is proposed which complements the previous models presented by Owen and co-workers [24,25].

2. Experimental

The aluminium rod electrodes were manufactured by galvanostatic electrodeposition of aluminium in the pores of a commercial polycarbonate (PC) membrane (Cyclopore, Whatman). The working and counter electrodes used in the electrodeposition step consisted of 500 μm thick aluminium plates (Goodfellow 99.999%) with 1 cm^2 areas. The working electrode, covered by a 200 nm pore size PC membrane (Cyclopore, Whatman), a glass fibre separator (Whatman) and the counter electrode were clamped together and immersed in an ionic liquid electrolyte consisting of 1-ethyl-3-methylimidazolium chloride (Alfa Aesar, >98%) and aluminium chloride (Alfa Aesar, 99.999%) in a 1:2 molar ratio. The galvanostatic deposition was carried out in an argon filled glove box (O_2 and H_2O < 2 ppm) as has been described elsewhere [32]. At the end of the deposition, the PC membrane was dissolved in dichloromethane (Sigma–Aldrich, 99.8%) for at least 30 min, resulting in self-supported aluminium rods on an aluminium substrate.

The 30 and 60 nm thick oxide layers were obtained by anodisation of the aluminium rod electrode employing a three-electrode cell, in which the Al nanorod electrode was used as the working electrode, a platinum coil served as the counter electrode and a Ag/AgCl electrode was used as the reference electrode. The anodisation, which was carried out in a 1 M KNO_3 (Merck, 99%) aqueous solution, was based on the number of cyclic voltammetric scans between 0 and +1 V vs. Ag/AgCl (at a scan rate of 1 mV s^{-1}) required to obtain the oxidation charges corresponding to the desired alumina layer thicknesses (i.e. 0.67 and 1.34C for 30 and 60 nm, respectively).

Li-ion cells were assembled in polymer laminated pouch cells inside an argon filled glove box with oxygen and water levels lower than 2 ppm. The aluminium nanorod working electrode and the combined counter and reference lithium electrode were separated

by a glass fibre separator (Whatman) soaked in an electrolyte containing 1 M LiFSI dissolved in EC:DEC (1:2). The cells were cycled employing cyclic voltammetry in a potential window between either 0.1 and 3.0 V or 0.1 and 1.0 V vs. Li^+/Li at a scan rate of 1 mV s^{-1} employing a VMP (BioLogic) potentiostat. Experiments involving combined chronoamperometric and linear scan voltammetric experiments were also performed. The morphology of the aluminium nanorod electrode was investigated by scanning electron microscopy (SEM) using a Zeiss 1550 scanning electron microscope. Transmission electron microscopy (TEM) was carried out using a JEOL JEM-2100 field-emission microscope operated at 200 kV. Bright-field TEM (BF-TEM) images were recorded by a CCD camera (Gatan Ultrascan 1000).

3. Results and discussion

To investigate the influence of the thickness of the alumina layer on the cycling stability of aluminium electrodes in Li-ion batteries, aluminium nanorod electrodes coated with 30 or 60 nm thick alumina layers were prepared by oxidation in 1 M KNO_3. In Fig. 1a, which shows a TEM image of an anodized aluminium nanorod electrode, it is seen that the total diameter of the nanorod was around 200 nm, in good agreement with the diameter of the pristine aluminium nanorod prior to the anodisation process. The thickness of the alumina shell can be seen to be about 60 nm, which together with the charge passed in the anodisation process indicate that the area gain for the used 3D aluminium substrates was approximately ten. A closer look at the alumina/aluminium interface also indicates that the anodisation process resulted in a significant roughening of the alumina/aluminium interface while the outer alumina surface of the pillar remained smooth. The selected-area electron diffraction (SAED) pattern for a part of the aluminium electrode is shown in Fig. 1b. It is clearly seen that the selected region of the aluminium electrode was a single crystal oriented close to a zone axis. The result is consistent with the BF-TEM image shown in Fig. 1a, in which the core of the electrode has dark contrast. In the SAED pattern diffuse scattering is observed, indicating the presence of an amorphous region in the electrode, which can be attributed to the alumina shell.

Fig. 2 shows cyclic voltammograms obtained for the aluminium nanorod electrodes with a native alumina layer as well as 30 and 60 nm thick alumina layers obtained by anodising the nanorods in 1 M KNO_3. The voltammograms were recorded between 0.1 and 3.0 V vs. Li^+/Li at a scan rate of 1 mV s^{-1} employing a combined lithium counter and reference electrode. As seen in Fig. 2, the voltammograms for all the three electrodes are dominated by a reduction peak at about 0.2 V vs. Li^+/Li and an oxidation peak at approximately 0.5 V vs. Li^+/Li. These peaks can be ascribed to the reduction of Li^+ yielding a LiAl alloy (i.e. $Li^+ + e^- + Al = LiAl$) and the corresponding oxidation of the alloy, since the standard potential for the alloy formation is about 0.4 V vs. Li^+/Li [25]. The similar voltammograms obtained for the three electrodes with different alumina thicknesses in Fig. 2 also suggest that the alumina layers merely acted as a lithium ion conducting membrane, since a significant reduction of the alumina coatings should have resulted in reduction currents proportional to the thickness of the alumina layers. Although the reduction charges were about four times larger for the anodised electrodes, it is unlikely that this was due to an increased reduction of alumina since no significant difference was seen between the reduction charges for the electrodes coated with 30 and 60 nm alumina layers. It should, however, be pointed out that it would be difficult to detect the presence of partial reduction of the alumina layer since the generated aluminium nanoparticles would undergo rapid LiAl alloy formation since the standard potential for the Al_2O_3 conversion reaction (i.e. $Al_2O_3 + 6Li^+ + 6e^- = 2Al + 3Li_2O$) is approximately 0.14 V vs. Li^+/Li. A larger aluminium surface area obtained as a result of the anodisation process (see Fig. 1) or large amounts of water absorbed in the thicker alumina layers therefore constitute more likely explanations for the larger reduction charges seen for the anodised samples. Although the two reduction peaks at about 1.25 and 0.45 V vs. Li^+/Li on the first cycle for the aluminium nanorod electrode with the native oxide layer (see Fig. 2a) could be ascribed to irreversible reduction of water and electrolyte to yield a solid electrolyte interphase (SEI) layer, respectively, a closer look at the currents on the first cathodic scan, however, also indicates the presence of slightly larger currents in the potential region between 2.0 and 0.2 V vs. Li^+/Li for the electrode with native oxide. The latter is not in agreement with the water reduction theory even though the results of additional experiments indicate that the reproducibility of the currents in this potential region was too poor to support any clear conclusion regarding the water reduction effect. Similar reduction peaks could be seen for the anodised electrodes although this is not clearly seen in Fig. 2 due to the different current scales used.

Small oxidation peaks at about 1.0 and 2.2 V vs. Li^+/Li which possibly could be associated with the reduction peaks at 0.45 and 1.25 V could also be seen on the first oxidation cycle for all the three electrodes (see Fig. 2). These oxidation peaks, which may originate from an oxidation of some of the species formed as a result of the reduction of water or electrolyte, were also most pronounced for the electrode with the native alumina coating. Since an

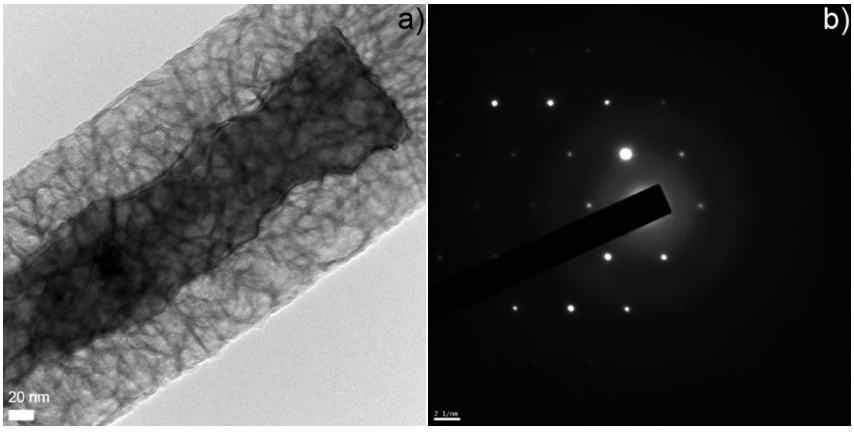

Fig. 1. a) BF-TEM image of an anodised aluminium rod with an approximately 60 nm thick alumina layer. b) SAED pattern of the same rod.

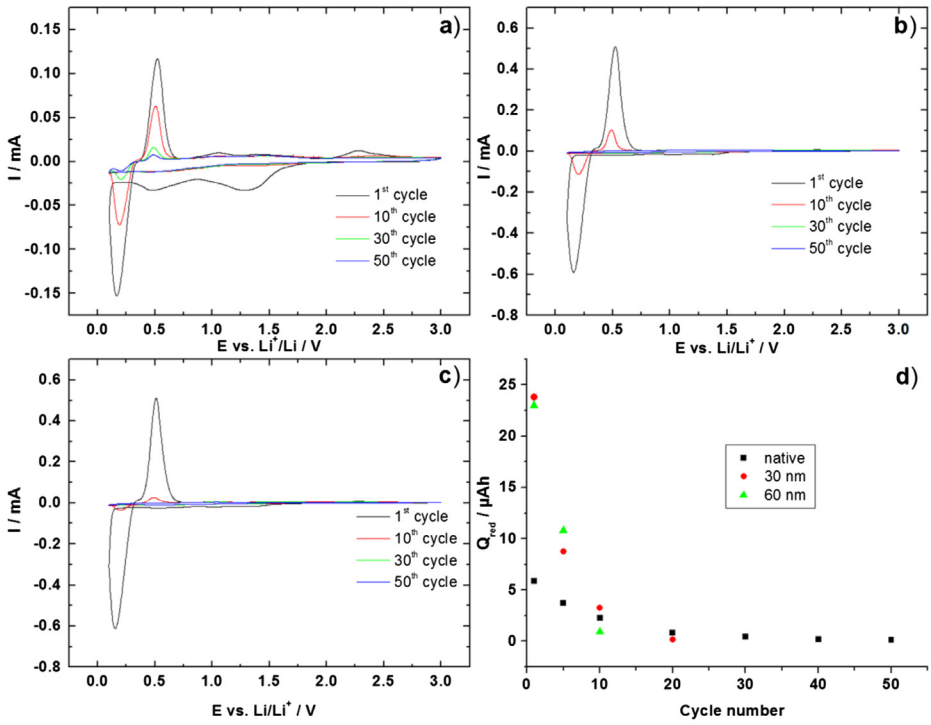

Fig. 2. Cyclic voltammograms recorded at a scan rate of 1 mV s^{-1} between 3.0 and 0.1 V vs. Li^+/Li for aluminium nanorod electrodes with a native (a), 30 nm (b) and 60 nm (c) alumina layer, respectively, as well as a plot of the reduction peak charges as a function of the cycle number (d). Note the different current scale in the a) figure as compared to in the b) and c) figures.

investigation of the origin of these additional first cycle reduction and oxidation peaks are outside the scope of this work the following discussion will be focused on the peaks due to the LiAl alloy formation and dealloying reactions.

From the nucleation loops in Fig. 2 it can clearly be seen that Li^+ reduction (i.e. the alloy formation reaction) was associated with a nucleation overpotential for all three electrodes on each scan. As this implies that this overpotential was independent of the scan history as well as the thickness of the alumina layer, it can be concluded that the electrode surface was completely stripped of LiAl during the anodic scan, in good agreement with the narrow and symmetric shape of all the oxidation peaks (see Fig. 2). The very similar lithium deposition results for all the three alumina thicknesses clearly show that the diffusion of Li^+ through the alumina layer was sufficiently fast not to affect the rate of the reduction reaction. This is not surprising as a diffusion coefficient for Li^+ in Al_2O_3 of the order of 10^{-14} cm^2 s^{-1} would be sufficient for these thin alumina layers.

Fig. 2d presents the reduction peak charges as a function of the cycle number for the three different aluminium electrodes (similar plots were also found for the oxidation peak charges and the total reduction charges as a function of cycle number as is seen in the Supporting Information). It is clearly seen that the reduction (i.e. alloy formation) charges decreased continuously upon cycling for all the electrodes. An analogous behaviour was also seen for the oxidation peak charges (see the Supporting Information). For the electrodes with 30 and 60 nm alumina layers, the lithium reduction peak was not distinguishable from the background after approximately 20 cycles. The peak charge after 50 cycles for the electrode with the native oxide layer was likewise negligible, exhibiting a value of less than 1 µAh. Similar results have been obtained by Au et al. [12] and Sharma and co-workers [13], who observed rapid capacity fading for aluminium nanorod electrodes during cycling between 0.1 and 3 V vs. Li^+/Li. In addition, the present results thus indicate that the capacity loss effect was more rather than less pronounced in the presence of a thicker alumina layer on the electrode. The latter is not in agreement with the expectations based on the mechanically supporting effects of such alumina layers. As discussed in the introduction, the loss of capacity seen in Fig. 2d could stem from either volume expansion effects or a loss of lithium in the aluminium electrodes. Based on the similar behaviour seen for the three electrodes with the different alumina thicknesses, it thus seems unlikely that these losses were due to volumetric effects, particularly as alumina layers are well known [30,31] to stabilise alloy forming electrodes. It is also difficult to understand why volume expansion effects would result in the continuous capacity fading upon cycling depicted in Fig. 2d.

To further study the capacity loss effects, experiments were carried out in a conventional electrochemical cell containing 15 mL of electrolyte using an aluminium nanorod working electrode coated with a native alumina layer and two lithium foils serving as the counter and reference electrodes, respectively. As can be seen in Fig. 3a, the obtained results were similar to those found with the Li-ion pouch cell which clearly shows that the rapid capacity fading during the cycling and the low coulombic efficiencies seen for the first few scans could not have been due to the depletion of Li^+ in the electrolyte or to a failure of the pouch cell as a result of volumetric expansion effects. As is seen in Fig. 3b, depicting a SEM image of the aluminium electrode obtained after the cycling experiments shown in Fig. 3a, the nanorod electrode was also found to be practically unaffected by the cycling experiments apart from a roughening of the pillars surface (SEM images for pristine aluminium can be found in our previous publication [32]). The latter is not unexpected considering that the experiments involved successive alloying and dealloying reaction which should lead to significant restructuring of the electrode surface. Based on the results shown in Fig. 3, it can therefore be concluded that the volume changes taking place during the first 60 cycles did not lead to any significant degradation of

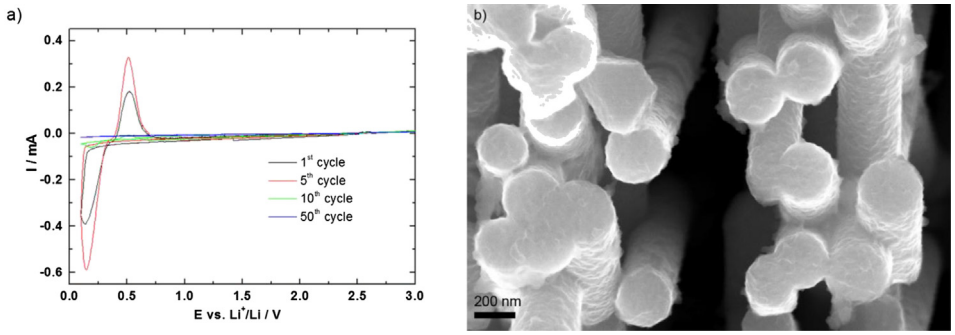

Fig. 3. Cyclic voltammograms, recorded at a scan rate of 1 mV s^{-1} between 3.0 and 0.1 V vs. Li^+/Li for an aluminium nanorod electrode coated with a native alumina layer obtained with a conventional three-electrode set-up in the presence of a large excess of the electrolyte (a) and a SEM image of the electrode after 60 cycles (b).

the nanorods. Unlike in the experiments depicted in Fig. 2, the reduction and oxidation peak charges in Fig. 3 were, however, found to increase rather than decrease during the first few cycles. After the fifth cycle, the peak charges, nevertheless, decreased continuously with increasing cycle number in accordance with the behaviour seen in Fig. 2. This indicates that the peak charges are affected by at least two phenomena, one which gives rise to an increase in the peak charges and one which causes the peak charges to decrease. These phenomena will be described in more detail below.

By comparing the shapes of the voltammograms in Figs. 2 and 3a, it can further be seen that both the reduction and oxidation peaks exhibit diffusion tails in the three-electrode experiment (see Fig. 3a), in good agreement with the expected semi-infinite diffusion behaviour. This indicates that both the deposition of lithium (yielding LiAl alloy) and the oxidation of the alloy are inherently diffusion controlled processes. A nucleation overpotential is likewise seen for all scans in Fig. 3a indicating that the oxidation of the alloy results in a full restoration of the aluminium surface at the aluminium/alumina interface also in this case.

In addition to the cyclic voltammetry experiments, pouch cell experiments were also carried out in which the aluminium electrode with native oxide layer was held at 0.15 V vs. Li^+/Li for different times (i.e., 10 and 20 min, respectively) after which the potential was linearly scanned to 3 V at a rate of 1 mV s^{-1}. The obtained chronoamperograms and linear scan voltammograms, some of which are presented in the Supporting Information, demonstrated that the oxidation charge always was about 90% of the reduction charge indicating that a part of the deposited lithium was lost into the aluminium electrode.

The present experimental results consequently indicate that the observed capacity decrease for the cycled aluminium nanorod electrodes was due to a loss of lithium in the aluminium electrodes along the lines suggested in the older aluminium electrode literature [15–29]. This would explain the low coulombic efficiencies seen on the first cycles for all the electrodes, irrespective of the alumina layer thickness, indicating that only a fraction of the deposited lithium (present as LiAl alloy) could be extracted from the electrode upon the oxidation. The nucleation behaviour observed on all reduction cycles further demonstrates that the deposition of lithium always took place on a pure aluminium surface. As it will be described below, this behaviour can readily be explained by a model in which it is assumed that the deposited lithium diffuses into the aluminium electrode during the reduction. As was very nicely described by Owen and co-workers [24,25] and as is further explained in Fig. 4, this gives rise to a layer of LiAl trapped between two aluminium (richer) layers as the oxidation starting from the LiAl/alumina interface regenerates the aluminium from its surface and inwards. This model is also in good agreement with the lithium concentration gradients within aluminium electrodes found by Ui et al. [29].

As is seen in Fig. 4, the lithium within the trapped LiAl layer will undergo diffusion not only in the direction towards the aluminium/alumina interface but also further into the aluminium electrode. It should be pointed out that this will be the case whenever the surface concentration of lithium is higher than that within the bulk of the aluminium electrode. As this situation is analogous to the diffusion profiles obtained as a result of a double chronoamperometric (or chronopotentiometric) step [33], it can be expected that the capacity loss effects should depend on the time domain of the experiment (i.e. the number of cycles used in the experiment). To test this, the reduction peak charges were plotted versus the inverse of the square root of the cycle number as is seen in Fig. 5 (note that the cycling time is proportional to the cycle number). It is clearly seen that a straight line was obtained for the electrode with the native oxide layer, indicating that the capacity loss indeed was

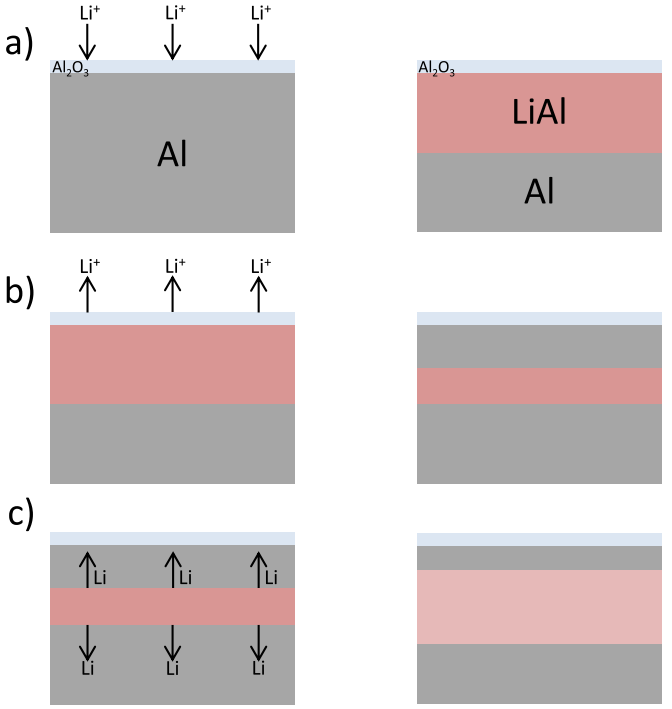

Fig. 4. Schematic representation of the alloying and dealloying processes for aluminium electrodes: a) lithium deposition yielding LiAl alloy formation, b) lithium oxidation resulting in a regeneration of the aluminium surface and c) two-way lithium diffusion within the aluminium electrode. For simplicity, the volumetric changes have not been included in the figure.

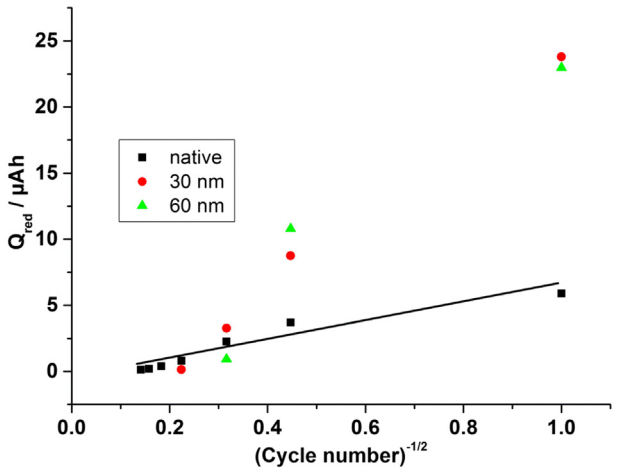

Fig. 5. Peak reduction charges (obtained from Fig. 2d) as a function of the inverse of the square root of cycle numbers for the aluminium electrodes with a native, 30 nm and 60 nm oxide layer, respectively. The solid line denotes a straight line fitted to the native oxide film data.

due to a diffusion controlled process. For the aluminium electrodes with 30 and 60 nm thick oxide layers, analogous linear relationships can be found but with larger slopes than for the native oxide layer. For the latter electrodes it was not possible to evaluate the reduction peak area for the later cycles which explains the absence of these points in Fig. 5 (see also Fig. 2d).

Another way of testing the model would be to use a different anodic potential limit than 3.0 V vs. Li^+/Li in the cycling experiments. Since the use of a more positive anodic limit than about 1 V would provide more time for the lithium diffusion effect, it should be possible to diminish the influence of the effect by shortening the time between the oxidation and the subsequent reduction (e.g. by using a lower anodic potential limit). It should be noted that the time spent in the alloy formation region should have no impact on the capacity loss due to the continuous formation of the alloy at these potentials. The fact that there was no oxidation current on the anodic scan for potentials more positive than about 0.8 V vs. Li^+/Li on the multicycle scans in Fig. 3 also shows that the diffusion rate of lithium through the aluminium layer on the surface of the electrode was very low. This means that the capacity loss as a result of the scanning to 3.0 V vs. Li^+/Li merely can be ascribed to time rather than potential effects. The combined chronoamperometric and linear scan experiments (see the Supporting Information) also support this conclusion.

In Fig. 6, cyclic voltammograms recorded with an anodic limit of 1.0 V rather than 3.0 V vs. Li^+/Li are shown. From the voltammograms and the plot of the reduction peak charges as a function of the number of cycles (see Fig. 6d) it can be observed that all the reduction peak charges in this case increased rather than decreased during the 100 cycles. Corresponding plots were also found for the oxidation peak charges as well as for the total charges as is seen in the Supplementary Data. The present results for the aluminium electrode are in agreement with the findings of Zein el Abedin et al. [11], who demonstrated a stable capacity for an aluminium nanowire electrode during four cycles between 0.01 and 1.1 V vs. Li^+/Li. Ui and co-workers [29] likewise showed that the charges obtained for the lithiation and delithiation of aluminium electrodes using cyclic voltammetry were larger for the 10th than for the first cycle. Although the latter authors used an oxidation cut-off potential of 2.5 V vs. Li^+/Li, their scan rate was five times higher than that used in the present study supporting the hypothesis that the capacity loss is coupled to the experimental time (at potentials more positive than that of the oxidation peak). In the present case, the reduction peak charges after 100 cycles were found to be about five times larger than the initial charges obtained for cycling up to 1.0 V vs. Li^+/Li. The present results therefore strongly indicate that the capacity loss can be circumvented by minimising the time during which the electrode is maintained at oxidising potentials.

As is seen in Fig. 6, the reduction peak charges for the 30 and 60 nm thick alumina layer electrodes were rather low for the first few cycles when compared to the ones for the electrode with the native alumina layer. As is more clearly seen in Fig. 6d, the capacity increase upon cycling thus appeared to be fastest for the electrode with the native oxide and slowest for the electrode with the 60 nm alumina layer (note that 60 nm alumina peak charge was always smaller than the 30 nm layer alumina peak charge). This phenomenon, which is not seen in Fig. 2 but which is present initially in Fig. 3, indicates that the electroactive amount of aluminium increased upon cycling and that this increase was hindered by a thicker alumina layer. The results also indicate that the reduction peak charges were approximately the same for all the electrodes after 100 cycles. It is therefore reasonable to assume that this phenomenon was coupled to an electrochemical milling effect due to the volume expansion associated with the alloying and dealloying reactions. Such effects were recently demonstrated [14] in a TEM study of the lithiation and delithiation of individual aluminium nanowires. These present results therefore indicate that the LiAl alloy and dealloying capacities are affected by two effects, the two-way diffusion of Li in the trapped LiAl layer in the electrode and an electromilling effect due to the volume changes associated with these electrodes, and that capacity decreases or increases can be obtained depending on the balance between these reactions. The latter explains the initial capacity increase, followed by the capacity decrease, seen in Fig. 3. This model is likewise in good agreement with the finding that the first cycle reduction peak charges were similar in Figs. 2 and 6 although the surface roughness effect for the anodise samples appears to be absent in the latter experiments.

From Fig. 6, it is evident that these voltammograms were more affected by iR drop effects than those depicted in Figs. 2 and 3 which can be explained by the larger currents as well as the expanded potential scale in Fig. 6. More importantly, a closer look at the oxidation peaks in the latter figure reveals the presence of a shoulder on the cathodic side of the oxidation peaks suggesting the existence of an additional oxidation reaction. Although the effect is not very pronounced, such a behaviour would be compatible with the presence of alloy nanoparticles formed by electromilling since it has been shown [34,35] that small metal particles are oxidised at significantly more negative potential than the corresponding particles of larger size.

The results presented in this work consequently demonstrate that the capacity decrease generally seen for the aluminium electrodes in Li-ion batteries mainly is due to a diffusion process involving the LiAl trapped within the aluminium electrode after the oxidation step while the volume expansion effects yielding electromilling in fact can give rise to a capacity increase upon cycling (at least for aluminium nanorods with a diameter of 200 nm coated with a native alumina layer or alumina layers with a thickness up to 60 nm). The effect of the lithium diffusion process will be larger when the electrode is maintained at oxidising potentials (i.e. at potentials more positive than about 0.3 V vs. Li^+/Li in the present case) for long periods of time since no Li deposition takes place at these potentials. The dramatic capacity loss seen when cycling to 3.0 V vs. Li^+/Li (see Fig. 2) is thus due to the increased time available for lithium diffusion within the aluminium electrode giving rise to a thicker but less concentrated alloy layer (see Fig. 4c). As the thickness of the electroactive layer of aluminium available at the

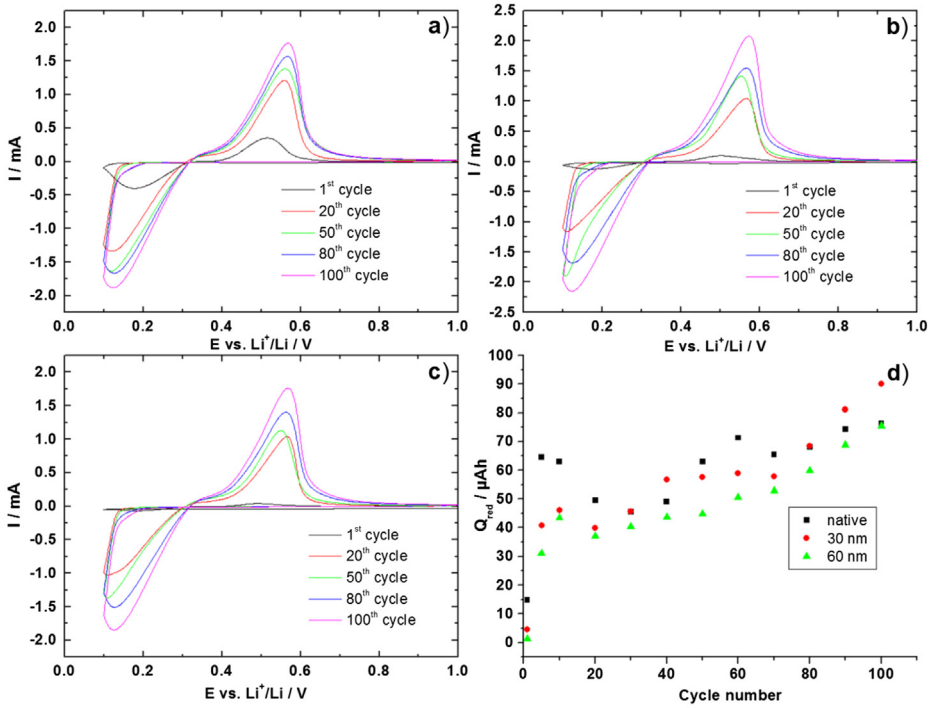

Fig. 6. Cyclic voltammograms recorded at a scan rate of 1 mV s^{-1} between 1.0 and 0.1 V vs. Li^+/Li for aluminium nanorod electrodes with a native (a), 30 nm (b) and 60 nm (c) alumina layer as well as the reduction peak charges as a function of the cycle number (d).

alumina interface is decreased, the second cycle reduction charge will be significantly smaller than the first and there will be a continuous capacity loss on each cycle until a steady-state situation is reached. Upon cycling to 1.0 (rather than 3.0) V vs. Li^+/Li, the effects of the lithium diffusion within the electrode is minimised due to the shorter period of time spent at oxidising potentials and a capacity increase is instead seen as a result of electromilling process associated with the volume changes inherent in the alloying and dealloying processes. The latter enables a larger volume of the electrode to be accessed during the cycling which gives rise to a capacity increase upon cycling, the duration of which increases with increasing thickness of the alumina layer which thus mainly serves as a mechanically stabilising solid electrolyte layer.

Although an Al_2O_3 conversion reaction is thermodynamically feasible at potentials more negative than about 0.14 V vs. Li^+/Li and a lithiation of alumina was indeed recently reported [14], the present study does not provide any convincing evidence for such a reaction. Since SEI formation should be possible, at least on native alumina layers, studies of the lithiation and delithiation of alumina layers should focus on the detection of the formation of aluminium (or LiAl) nanoparticles at the alumina/electrolyte interface. For native alumina layers this would unfortunately be complicated by the possibility of generating such particles by the lithiation and delithiation of the aluminium surface some nanometres below the native alumina layer.

4. Conclusions

The present results demonstrate that the capacity losses seen for aluminium nanorod electrodes, coated with a native alumina layer as well as 30 and 60 nm alumina layers obtained by anodisation and cycled between 3.0 and 0.1 V vs. Li^+/Li at a scan rate of 1 mV s^{-1}, were due to losses of lithium as a result of the formation of a trapped LiAl layer within the aluminium electrode. Based on a model complementing previous models in the literature, it is proposed that the lithium within the latter LiAl layer undergoes a diffusion process leading to a continuous loss of lithium predominantly during the first 20 cycles after which a steady state capacity is reached. It is also demonstrated that a capacity increase was seen when the cycling was carried out between 1.0 (rather than 3.0) and 0.1 V vs. Li^+/Li due to the decreased lithium diffusion effect and an increase in the electroactive fraction of the aluminium electrode caused by the electromilling associated with the volume changes due to the alloying and dealloying reactions. The capacity increase was found to extend over at least 100 cycles for the electrodes with 30 and 60 nm alumina layers most likely due to the increased mechanical stability provided by these layers in comparison with that for the much thinner native alumina layer. No significant improvement of the cycling performance of the electrodes was found when increasing the alumina layer beyond the thickness of the native layers in good agreement with the conclusion that the capacity retention mainly depends on the extent of the loss of lithium within the aluminium electrode. It is thus concluded that the origin of the capacity fading for the present aluminium nanorod electrodes is the diffusion of lithium into the aluminium electrode, and not a pulverisation of the electrode caused by the volume changes associated with the alloying and dealloying processes, in contrast with contemporary beliefs but in excellent agreement with the conclusions presented in older studies.

Acknowledgements

The authors are grateful for financial support from The Swedish Research council (VR) (project number 2011-3506) and The Ångström Advanced Battery Center (ÅABC) (project number 2012-4681) as well as from StandUp for Energy and The Swedish Energy Agency (STEM). The Knut and Alice Wallenberg Foundation is likewise acknowledged for an equipment grant for the electron microscopy facilities at Stockholm University. Fruitful discussions with Dr. Mario Valvo are greatly appreciated.

Appendix A. Supplementary data

Supplementary data related to this article can be found at http://dx.doi.org/10.1016/j.jpowsour.2014.06.118.

References

[1] A.N. Dey, J. Electrochem. Soc. 118 (1971) 1547–1549.
[2] C.M. Park, J.H. Kim, H. Kim, H.J. Sohn, Chem. Soc. Rev. 39 (2010) 3115.
[3] Y. Hamon, T. Brousse, F. Jousse, P. Topart, P. Buvat, D.M. Schlech, J. Power Sources 97-98 (2001) 185–187.
[4] N.S. Hudak, D.L. Huber, J. Electrochem. Soc. 159 (2012) A688–A695.
[5] X. Lei, C. Wang, Z. Yi, Y. Liang, J. Sun, J. Alloys Comp. 429 (2007) 311–315.
[6] N. Kumagai, K. Kikuchi, K. Tanno, J. Appl. Electrochem 22 (1992) 620–627.
[7] L.H.S. Gasparotto, A. Prowald, N. Borisenko, S. Zein El Abedin, A. Garsuch, F. Endres, J. Power Sources 196 (2011) 2879–2883.
[8] J.O. Besenhard, M. Hess, P. Komenda, Solid State Ion 40/41 (1990) 525–529.
[9] C.Y. Wang, Y.S. Meng, G. Ceder, Y. Li, J. Electrochem. Soc. 155 (2008) A615–A622.
[10] X. Lei, J. Ma, Mater. Chem. Phys. 116 (2009) 383–387.
[11] S. Zein El Abedin, A. Garsuch, F. Endres, Aust. J. Chem. 65 (2012) 1529–1533.
[12] M. Au, S. McWhorter, H. Ajo, T. Adams, Y. Zhao, J. Gibbs, J. Power Sources 195 (2010) 3333–3337.
[13] S.K. Sharma, M.-S. Kim, D.Y. Kim, J.-S. Yu, Electrochim. Acta 87 (2013) 872–879.
[14] Y. Liu, N.S. Hudak, D.L. Huber, S.J. Limmer, J.P. Sullivan, J.Y. Huang, Nano Lett. 11 (2011) 4188–4194.
[15] B.M.L. Rao, R.W. Francis, H.A. Christopher, J. Electrochem. Soc. 124 (1977) 1490–1492.
[16] E.J. Frazer, J. Electroanal. Chem. 121 (1981) 329–339.
[17] J.O. Besenhard, J. Electroanal. Chem. 94 (1978) 77–81.
[18] I. Epelboin, M. Froment, M. Garreau, J. Thevenin, D. Warin, J. Electrochem. Soc. 127 (1980) 2100–2104.
[19] Y. Geronov, P. Zlatilova, R.V. Moshtev, J. Power Sources 12 (1984) 145–153.
[20] A.S. Baranski, W.R. Fawcett, T. Krogulec, M. Dragowska, J. Electrochem. Soc. 131 (1984) 1750–1755.
[21] P. Zlatilova, I. Balkanov, Y. Geronov, J. Power Sources 24 (1988) 71–79.
[22] M. Garreau, J. Thevenin, M. Fekir, J. Power Sources 9 (1983) 235–238.
[23] Y. Geronov, P. Zlatilova, G. Staikov, Electrochim. Acta 29 (1984) 551–555.
[24] J.R. Owen, W.C. Maskell, B.C.H. Steele, T.S. Nielsen, O.T. Sørensen, Solid State Ion 13 (1984) 329–334.
[25] W.C. Maskell, J.R. Owen, J. Electrochem. Soc. 132 (1985) 1602–1607.
[26] Y. Geronov, P. Zlatilova, G. Staikov, J. Power Sources 12 (1984) 155–165.
[27] T.R. Jow, C.C. Liang, J. Electrochem. Soc. 129 (1982) 1429–1434.
[28] A.S. Baranski, W.R. Fawcett, J. Electrochem. Soc. 129 (1982) 901–907.
[29] K. Ui, K. Yamamoto, K. Ishikawa, T. Minami, K. Takeuchi, M. Itagaki, K. Watanabe, N. Koura, J. Power Sources 183 (2008) 347–350.
[30] L.A. Riley, A.S. Cavanagh, S.M. George, Y.S. Jung, Y. Yan, S.-H. Lee, A.C. Dillon, ChemPhysChem 11 (2010) 2124–2130.
[31] Y. He, X. Yu, Y. Wang, H. Li, X. Huang, Adv. Mater. 23 (2011) 4938–4941.
[32] G. Oltean, L. Nyholm, K. Edström, Electrochim. Acta 56 (2011) 3203–3208.
[33] A.J. Bard, L.R. Faulkner, Electrochemical Methods, second ed., Wiley, New York, 2001.
[34] R.A. Masitas, F.P. Zamborini, J. Am. Chem. Soc. 134 (2012) 5014–5017.
[35] P.L. Redmond, A.J. Hallock, L.E. Brus, Nano Lett. 5 (2005) 131–135.